frontiers in
ENERGY RESEARCH

ORIGINAL RESEARCH ARTICLE
published: 31 October 2014
doi: 10.3389/fenrg.2014.00048

Ion beam irradiation-induced amorphization of nano-sized $K_xLn_yTa_2O_{7-v}$ tantalate pyrochlore

Fengyuan Lu[1,2], Yiqiang Shen[1,3], Zhili Dong[3], Gongkai Wang[1], Fuxiang Zhang[4], Rodney C. Ewing[5] and Jie Lian[1]*

[1] *Department of Mechanical, Aerospace and Nuclear Engineering, Rensselaer Polytechnic Institute, Troy, NY, USA*
[2] *Department of Mechanical and Industrial Engineering, Louisiana State University, Baton Rouge, LA, USA*
[3] *School of Materials Science and Engineering, Nanyang Technological University, Singapore*
[4] *Department of Geological Sciences, University of Michigan, Ann Arbor, MI, USA*
[5] *Department of Geological and Environmental Sciences, Stanford University, Stanford, CA, USA*

Edited by:
Satoshi Utsunomiya, Kyushu University, Japan

Reviewed by:
Claudio Tenreiro, University of Talca, Chile
Satoshi Utsunomiya, Kyushu University, Japan
Ritesh Sachan, Oak Ridge National Laboratory, USA

****Correspondence:***
Jie Lian, Department of Mechanical, Aerospace and Nuclear Engineering, Rensselaer Polytechnic Institute, JEC 5048, 110 8th street, Troy, NY 12180, USA
e-mail: lianj@rpi.edu

Nano-sized (~10–15 nm) tantalate pyrochlores $K_xLn_yTa_2O_{7-v}$ (Ln = Gd, Y, and Lu) were irradiated with 1 MeV Kr^{2+} beams at different temperatures and their radiation response behaviors were studied by *in situ* transmission electron microscopy observations. All of these nano-sized $K_xLn_yTa_2O_{7-v}$ pyrochlores are sensitive to radiation-induced amorphization with low-critical doses (~0.12 dpa) at room temperature and high-critical amorphization temperatures above 1160 K. The K^+ plays a key role in determining the radiation response of tantalate pyrochlores, in which the K^+-rich $KLuTa_2O_7$ displays greater amorphization susceptibility than $K_{0.8}GdTa_2O_{6.9}$ and $K_{0.8}YTa_2O_{6.9}$ with lower K^+ occupancy at the A-site. The reduced amorphization tolerance of the composition with a greater K^+ content is consistent with the prominently larger K^+/Ta^{5+} cationic radius ratio, which may result in more structural deviation from the parent fluorite structure and less capability to accommodate radiation-induced defects. An empirical correlation between critical amorphization temperature and ionic size was derived, generally describing the dominant effect of the cation ionic size in controlling radiation response of a wide range of pyrochlore compounds as potential nuclear waste forms. The results of the tantalate pyrochlore in this work highlight that nanostructured pyrochlores are not intrinsically radiation tolerant and their responses are highly compositional dependent.

Keywords: nanostructured pyrochlore, radiation tolerance, nuclear waste forms, ion beam-induced amorphization

INTRODUCTION

The $A_2B_2O_7$ pyrochlore with a cubic structure of *Fd*-3*m* space group is a derivative of the fluorite structure but with two cation sites and one eighth of the anions absent. The A and B cation sites of $A_2B_2O_7$ pyrochlores can accommodate a wide variety of metal elements, resulting in more than 500 compositions. With further loss of anions, the structure can become a defect pyrochlore structure of $A_2B_2O_6$. The $A_2B_2O_7$ pyrochlores exhibit high-chemical durability, excellent compatibility with actinides, and tunable radiation tolerance by controlling their cationic compositions and electronic bonding, and therefore, are considered as important host materials for nuclear waste forms and fuel matrix (Raison et al., 1999; Ewing et al., 2004). The radiation stability of pyrochlores can be greatly affected by their cationic compositions. One classical example is that the pyrochlore radiation resistance can be improved dramatically by substituting the Ti^{4+} cations in the $Gd_2Ti_2O_7$ pyrochlore with Zr^{4+} cations, which results in a smaller A site to B site cation ionic radius ratio (r_A/r_B), and amorphization cannot be reached in $Gd_2Zr_2O_7$ even at an extremely high-damage level up to 100 dpa at room temperature (Wang et al., 1999). The discovery of the radiation-resistant materials based on pyrochlore structure-type has significant environmental impacts on effective nuclear waste management, critical for developing advanced nuclear energy systems. The fundamental physics governing the phase and structural stability under intensive radiation conditions is critical for designing radiation tolerant materials. Extensive research activities on pyrochlore materials are ongoing from both experimental and atomistic modeling perspectives, revealing the importance of cation ionic size, structural disorder, and electronic structure in controlling the radiation performance of pyrochlore materials (Lian et al., 2002, 2003; Patel et al., 2008; Zhang et al., 2009a,b, 2010). Specifically, the smaller ionic radius ratio of A-site to B-site will lead to less structural deviation from the parent fluorite structure and thus a greater tendency toward an order-disorder structural transition from pyrochlore to fluorite upon intensive radiations due to the lower formation energies of cation anti-site defects. As a result, materials become more radiation tolerant (Sickafus et al., 2000).

Recently, for the purpose of mitigating the radiation damage, nano-scale materials design strategy has been applied in order to develop advanced nuclear materials with enhanced radiation performance. The rationale is that nanostructured materials are more radiation resistant as the high densities of surfaces, interfaces, and grain boundaries may behave as sinks for defect recovery. The enhanced radiation performance was demonstrated by previous studies on spinel, TiN, and ZrO_2 (Rose et al., 1995, 1997;

Shen et al., 2007; Wang et al., 2007). It was also reported that the radiation performance of nano-sized pyrochlores with a composition of $Gd_2(Ti_{0.65}Zr_{0.35})_2O_7$ increases drastically as the grain size decreases below 20 nm (Zhang et al., 2009a,b). As compared with zirconate (Wang et al., 1999; Lian et al., 2002; Ewing et al., 2004; Patel et al., 2008), titanate (Lian et al., 2003; Patel et al., 2008), and stannate (Lian et al., 2006) pyrochlores, nano-sized tantalate pyrochlores have not been studied previously, and no experimental data are available for understanding the impact of their cationic compositions on their radiation stability. In this study, we investigate the response of nano-sized $K_xLn_yTa_2O_{7-v}$ pyrochlores (Ln = Y, Gd, Lu) under intensive radiation environments. Our results indicate that tantalate pyrochlores with average grain sizes of ~10–15 nm are radiation sensitive with high-critical amorphization temperatures and the potassium occupancy at the pyrochlore A-site significantly affects materials resistance against radiation-induced amorphization. These results also highlight that nanostructured pyrochlores are not intrinsically radiation tolerant and their radiation performance is highly compositional dependent.

EXPERIMENTAL

The rare earth-doped tantalate pyrochlores of $K_xLn_yTa_2O_{7-v}$ used in this study were synthesized in Sandia National laboratory using hydrothermal methods upon aqueous reaction between K^+-salts of the $[Ta_6O_{19}]^{8-}$ polyoxometalate ion and lanthanide citrate complexes at 220 °C (Nyman et al., 2009). A PANalytical X'pert Pro X-ray diffractometer was used for X-ray diffraction (XRD) characterization, and the Rietveld refinement was performed in TOPAS program (Version 3.0 Bruker AXS, Karlsruhe, Germany) to determine the structures and phase compositions of these pyrochlores. Quantitative energy-dispersive X-ray spectra (EDS) were collected at random locations of each sample and analyzed statistically in order to provide complementary information on the chemical compositions of the tantalate pyrochlores. Transmission electron microscopy (TEM) characterization was conducted using a Hitachi H-9000NAR TEM with 300 KeV electron beam.

The ion irradiation experiments were conducted using the IVEM-tandem facility at Argonne National Laboratory, which combines a Hitachi H-9000NAR TEM with an NEC Tandem ion accelerator, enabling *in situ* TEM observation of material behaviors under intensive ion bombardment. A heating stage equipped with the TEM allows irradiation experiments in a wide temperature range from 300 to 1023 K. The $K_xLn_yTa_2O_{7-v}$ nanoparticles were irradiated with 1 MeV Kr^{2+} ions at an ion flux of 6.25×10^{11} ions/cm^2 and their microstructural evolution was monitored *in situ* by selected area electron diffraction (SAED) and dark field TEM imaging. The dark field imaging was obtained by inserting an objective aperture to cover the low-index diffraction rings of the SAED. The ion species and energy chosen for the irradiation were aimed at simulating the radiation effects of alpha decay on $K_xLn_yTa_2O_{7-v}$. The critical amorphization fluences were obtained when diffraction rings completely faded and amorphous halos appeared in the SAED patterns. The full cascade calculations using SRIM 2008 program were performed in order to convert the critical fluence to a universal damage unit of dpa.

RESULTS AND DISCUSSION

MATERIALS CHARACTERIZATION

The crystal structures of the three different samples are characterized by XRD and the patterns are compared side by side in **Figure 1**. The XRD pattern of the Gd^{3+}-doped tantalate pyrochlore fits a single-phase pyrochlore structure, whereas the Y^{3+} and Lu^{3+}-doped tantalate pyrochlores exhibit peak-doublings at 2-Theta positions of around 29°, 34°, 49°, 58°, suggesting that the existence of dual phases. Quantitative EDS analysis also reveals that the chemical composition of the Gd^{3+}-doped tantalate pyrochlore sample is uniform throughout the sample; whereas the Y^{3+} and Lu^{3+}-doped samples each shows two distinct chemical compositions with quite different K^+ contents, consistent with the XRD results. Accordingly, the EDS data are grouped into five phases, and their average chemical compositions in atom percentage are listed in **Table 1**.

Rietveld refinements of the XRD patterns were performed based on the nominal chemical compositions by EDS analysis. A 2-Theta range of 25°–70° was used due to the high background before 25°. The refinement results, as shown in **Table 2**, reveal that the Gd^{3+}-doped pyrochlore powders consist of a single phase as face-centered cubic (fcc) $K_{0.8}GdTa_2O_{6.9}$ with *Fd*-3*m* space group. In contrast, both Y^{3+}- and Lu^{3+}-doped samples consist of two different phases. Specifically, the Y^{3+}-doped samples consist of $K_{0.8}YTa_2O_{6.9}$ (27.2 wt%) and $K_{0.4}Y_{0.8}Ta_2O_{6.4}$ (72.8 wt%), and the Lu^{3+}-doped pyrochlore samples consist of $KLuTa_2O_7$ (12.8 wt%) and $K_{0.4}Lu_{0.8}Ta_2O_{6.4}$ (87.2 wt%), all being fcc structure with *Fd*-3*m* group space. As for the dual-phase Y^{3+} and Lu^{3+}-doped compounds, the *x* parameter of 48f oxygen is 0.332 for $K_{0.8}YTa_2O_{6.9}$ and 0.316 for $KLuTa_2O_7$, indicating that the structures are close to $A_2B_2O_7$ pyrochlore; in contrast, the *x* parameter is 0.305 for $K_{0.4}Y_{0.8}Ta_2O_{6.4}$ and 0.306 for $K_{0.4}Lu_{0.8}Ta_2O_{6.4}$, smaller than that of perfectly ordered pyrochlores ($x = 0.3125$) (Subramanian et al., 1983) indicating that these two phases are closer to the $A_2B_2O_6$ defect pyrochlore structure. The slight differences in lattice parameters between the two phases of Y^{3+} and Lu^{3+}-doped samples result in the doubling of peaks in XRD patterns as shown in **Figure 1**. However, the difference in the lattice parameter is too small ($\leq$0.05 Å) to be differentiated by electron diffractions in TEM. The morphology, crystal size, and microstructure of the $K_xLn_yTa_2O_{7-v}$ samples were further characterized by TEM. The TEM images in **Figure 2** show that these tantalate pyrochlores are in the form of nanoparticles with average particle sizes of ~10–15 nm, consistent with the XRD refinement results.

ION IRRADIATION-INDUCED AMORPHIZATION

The radiation damage in the $K_xLn_yTa_2O_{7-v}$ induced by 1 MeV Kr^{2+} bombardment was simulated in SRIM 2008 program using a chemical formula of $K_{0.8}GdTa_2O_{6.9}$ for the Gd-doped sample and the average chemical formulae of $K_{0.50}Y_{0.85}Ta_2O_{6.53}$ and $K_{0.47}Lu_{0.82}Ta_2O_{6.47}$ for the Y and Lu-doped dual-phase samples, respectively, and a displacement energy of 50 eV was applied to all the tantalate pyrochlores. The damage levels were given in dpa by converting the corresponding ion fluences based on the SRIM 2008 calculations, and the calculated nuclear and electron stopping powers are listed in **Table 3**. The nuclear stopping powers of each sample are higher than the corresponding

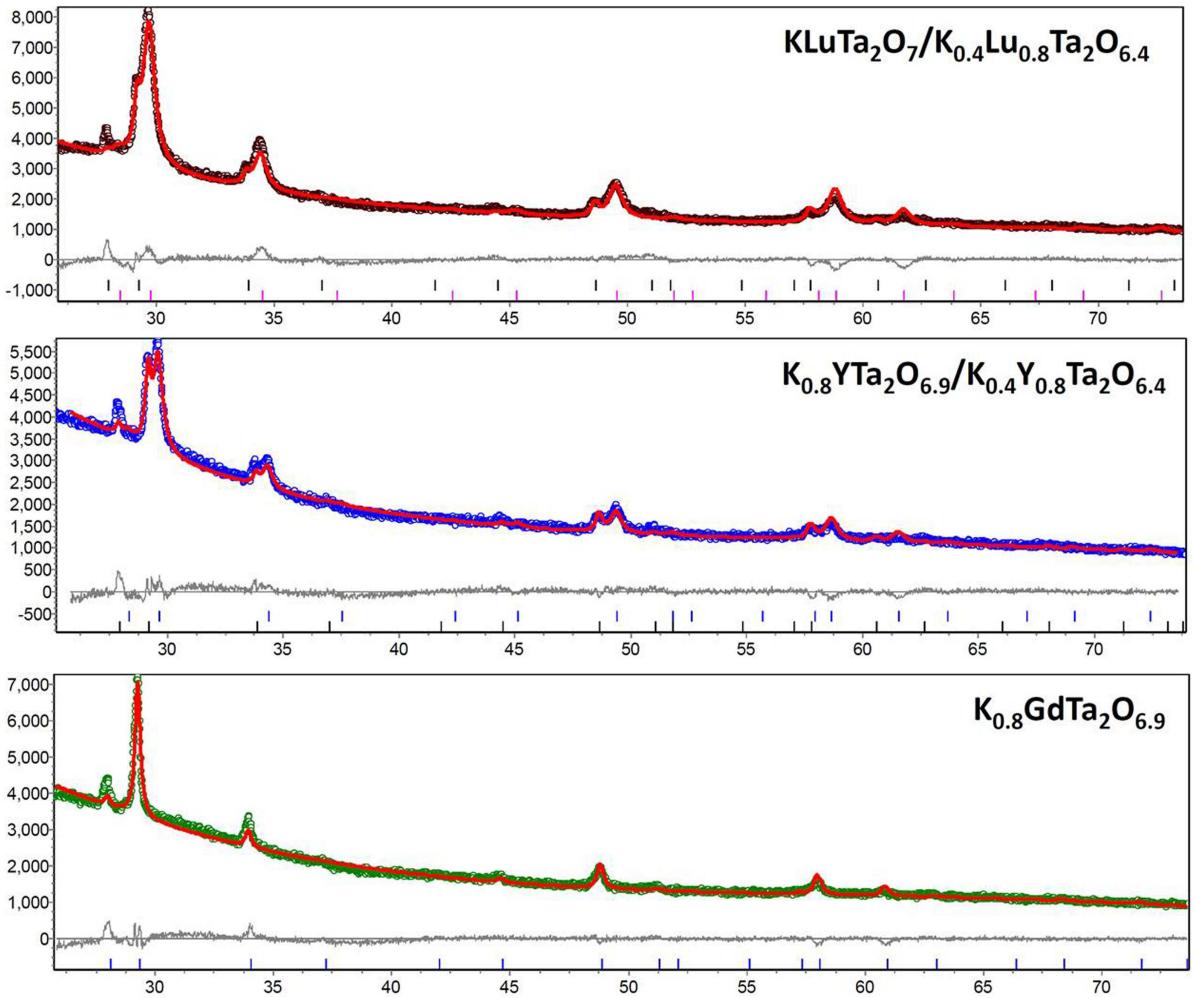

FIGURE 1 | (Color online) XRD patterns of nano-sized tantalate pyrochlore samples and the corresponding Rietveld refinement fittings. The *x*-axes are 2-Theta position and the *y*-axes are intensity in counts. The dual phases in the Lu^{3+}- and Y^{3+}-doped samples result in the doubling of peaks. The chemical compositions are determined by Rietveld refinement results.

Table 1 | EDS analysis of the tantalate pyrochlores give five different groups of chemical compositions, each with a distinct atomic percentage of cation composition.

		Y^{3+}-doped				Lu^{3+}-doped			
Gd^{3+}-doped		Phase 1		Phase 2		Phase 1		Phase 2	
Element	**Atomic %**	**Element**	**Atomic %**	**Element**	**Atomic %**	**Element**	**Atomic %**	**Element**	**Atomic %**
K	7.2	K	5.9	K	7.0	K	6.8	K	3.5
Gd	8.2	Y	11.9	Y	9.2	Lu	7.5	Lu	9.7
Ta	19.6	Ta	17.5	Ta	19.0	Ta	20.3	Ta	20.1
O	65.0	O	64.6	O	64.8	O	65.4	O	66.6

electron stopping powers, which suggests that the elastic collision may dominate the ion irradiation and create high-displacements defects in the materials. These displacement defects will contribute to the microstructural changes of the samples as the key factor.

As observed with *in situ* TEM, upon 1 MeV Kr^{2+} ion irradiations at room temperature, $K_{0.8}GdTa_2O_{6.9}$, $K_{0.8}YTa_2O_{6.9}/K_{0.4}Y_{0.8}Ta_2O_{6.4}$, and $KLuTa_2O_7/K_{0.4}Lu_{0.8}Ta_2O_{6.4}$ nanoparticles all undergo a crystalline-to-amorphous phase transformation. The

Table 2 | Rietveld refinement parameters of the nano-sized tantalate pyrochlore: nominal compositions, weight percentage of each phase, *x* parameter of oxygen 48f, related structure, lattice constant a (Å), *R* factors (R_{exp}, R_{wp}, R_p), and goodness of fit (χ^2).

	Gd^{3+}-doped	Y^{3+}-doped		Lu^{3+}-doped	
	$K_{0.8}GdTa_2O_7$	$K_{0.8}YTa_2O_{6.9}$	$K_{0.4}Y_{0.8}Ta_2O_{6.4}$	$KLuTa_2O_7$	$K_{0.4}Lu_{0.8}Ta_2O_{6.4}$
Wt%	100	27.2	72.8	12.8	87.2
x Parameter of oxygen 48f	0.318	0.332	0.305	0.316	0.306
Related structure	$A_2B_2O_7$	$A_2B_2O_7$	$A_2B_2O_6$	$A_2B_2O_7$	$A_2B_2O_6$
a (Å)	10.53	10.58	10.43	10.58	10.40
R_{exp}	2.37	2.37		2.30	
R_{wp}	3.57	4.04		4.77	
R_p	2.84	3.25		3.60	
χ^2	1.50	1.71		2.07	

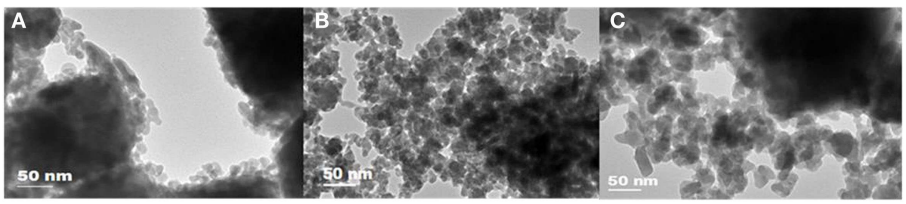

FIGURE 2 | Transmission electron microscopy images of (A) $K_{0.8}GdTa_2O_{6.9}$; (B) $K_{0.8}YTa_2O_{6.9}/K_{0.4}Y_{0.8}Ta_2O_{6.4}$; (C) $KLuTa_2O_7/K_{0.4}Lu_{0.8}Ta_2O_{6.4}$.

Table 3 | The nuclear stopping power (S_n) and electron stopping power (S_e) of the incident 1 MeV Kr^{2+} in different $K_xLn_yTa_2O_{7-v}$ samples; *x* parameters of oxygen 48f; critical amorphization doses at 300 and 873 K and the critical amorphization temperatures of the tantalate pyrochlores.

	$K_{0.8}GdTa_2O_{6.9}$	$K_{0.8}YTa_2O_{6.9}$/ $K_{0.4}Y_{0.8}Ta_2O_{6.4}$	$KLuTa_2O_7$/ $K_{0.4}Lu_{0.8}Ta_2O_{6.4}$
S_n (KeV/nm)	1.353	1.344	1.301
S_e (KeV/nm)	0.852	0.846	0.794
x Parameter of oxygen 48f	0.318	0.332/0.305	0.316/0.306
Critical dpa at 300 K	0.12	0.12	0.12
Critical fluence at 300 K (ions/cm^2)	2.5×10^{14}	2.5×10^{14}	2.5×10^{14}
Critical dpa at 873 K	0.30	0.30	0.14
Critical fluence at 873 K (ions/cm^2)	6.25×10^{14}	6.25×10^{14}	3×10^{14}
T_c (K)	1167 ± 41	1165 ± 34	~1291

in situ TEM dark field images and SAED patterns in **Figure 3** illustrate a similar room temperature ion beam-induced amorphization process of the three samples. The crystallinity of the original nanoparticles is indicated by the bright contrast in the dark field image and the diffraction ring patterns, characteristic for nanostructured tantalate pyrochlores (inset in **Figures 3A,D,G**). Upon 1 MeV Kr^{2+} irradiation with a dpa of 0.05, the contrast of the dark field images of all three samples was reduced gradually and the diffraction rings became vague as shown in **Figures 3B,E,H**. The nanoparticles were completely amorphized by 1 MeV Kr^{2+} at a critical dose of 0.12 dpa, as evidenced in **Figures 3C,F,I**. These results suggest that nano-sized tantalate pyrochlores are highly radiation sensitive and can be amorphized at a relatively low-damage level (~0.12 dpa).

A decrease in potassium content in the three pyrochlore samples was observed by post-irradiation quantitative EDS analysis. The average atomic percentage of potassium decreased from the original 7.2 to 3.5 at % in the irradiated $K_{0.8}GdTa_2O_{6.9}$, from 6.2 to 2.6 at % in $K_{0.8}YTa_2O_{6.9}/K_{0.4}Y_{0.8}Ta_2O_{6.4}$, and from 3.9 to 1.7 at % in $KLuTa_2O_7/K_{0.4}Lu_{0.8}Ta_2O_{6.4}$. The loss of potassium is likely due to increased release rate of the highly volatile potassium in the radiation-induced amorphous matrix as a result of volume changes, increased surface area, reduced atomic bonding constraints, changes in local coordination, and the pathways for ion exchange.

The critical amorphization doses of the three $K_xLn_yTa_2O_{7-v}$ samples all increase at elevated temperature. **Figure 4** shows their amorphization processes under 1 MeV Kr^{2+} at 873 K. As the ion irradiation-induced amorphization process is mainly a competition between the accumulation of defects upon radiation and the recovery process of these defects, elevated temperature will lead to the increase of defect mobility in the materials and consequently the enhanced dynamics for defect annealing. As a result, the critical amorphization dose increases with temperature. It is also noted that the critical doses of $K_{0.8}GdTa_2O_{6.9}$, $K_{0.8}YTa_2O_{6.9}/K_{0.4}Y_{0.8}Ta_2O_{6.4}$, and $KLuTa_2O_7/K_{0.4}Lu_{0.8}Ta_2O_{6.4}$ are similar at room temperature, but differentiate at elevated

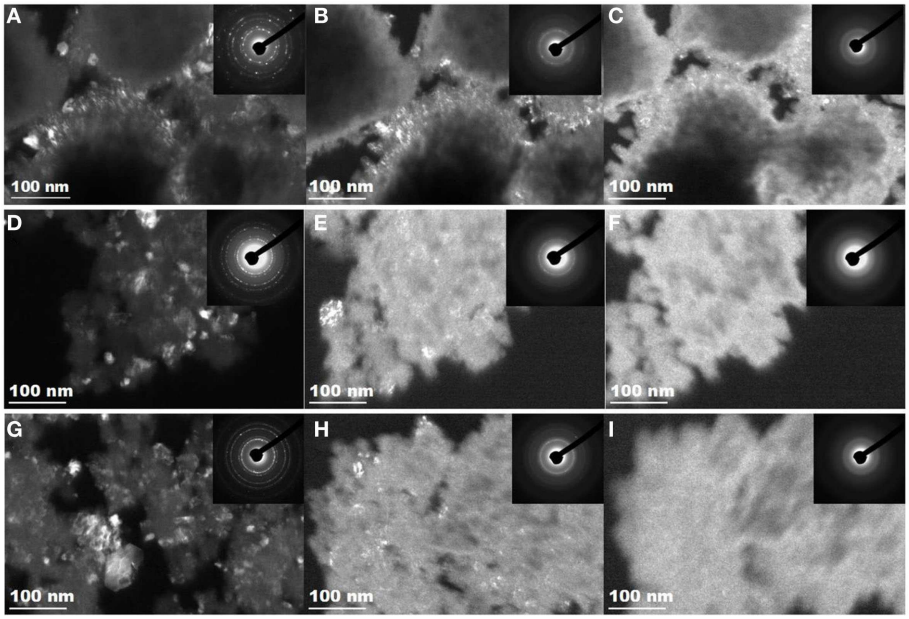

FIGURE 3 | Transmission electron microscopy dark field images and SAED patterns show the 1 MeV Kr^{2+} irradiation-induced amorphization process of the nano-sized tantalate pyrochlores at room temperature. Irradiation process of $K_{0.8}GdTa_2O_{6.9}$: **(A)** unirradiated, **(B)** 0.05 dpa (1×10^{14} ions/cm^2), **(C)** amorphized at 0.12 dpa (2.5×10^{14} ions/cm^2); irradiation process of $K_{0.8}YTa_2O_{6.9}/K_{0.4}Y_{0.8}Ta_2O_{6.4}$: **(D)** unirradiated, **(E)** 0.05 dpa (1×10^{14} ions/cm^2), **(F)** amorphized at 0.12 dpa (2.5×10^{14} ions/cm^2); irradiation process of $KLuTa_2O_7/K_{0.4}Lu_{0.8}Ta_2O_{6.4}$: **(G)** unirradiated, **(H)** 0.05 dpa (1×10^{14} ions/cm^2), **(I)** amorphized at 0.12 dpa (2.5×10^{14} ions/cm^2).

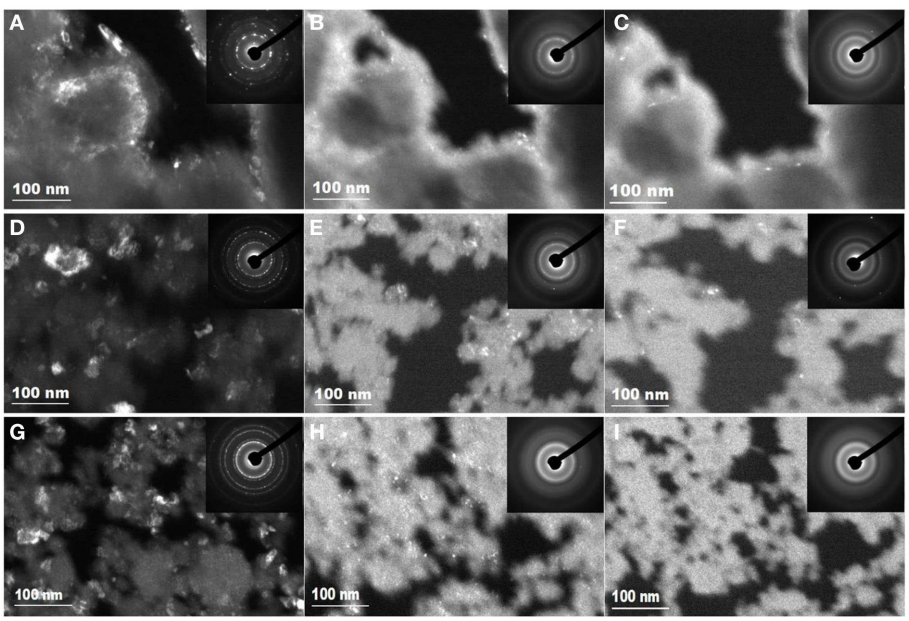

FIGURE 4 | Transmission electron microscopy dark field images and SAED patterns show the 1 MeV Kr^{2+} irradiation-induced amorphization process of the nano-sized tantalate pyrochlores at 873 K. Irradiation process of $K_{0.8}GdTa_2O_{6.9}$: **(A)** unirradiated, **(B)** 0.10 dpa (2×10^{14} ions/cm^2), **(C)** amorphized at 0.30 dpa (6.25×10^{14} ions/cm^2); irradiation process of $K_{0.8}YTa_2O_{6.9}/K_{0.4}Y_{0.8}Ta_2O_{6.4}$: **(D)** unirradiated, **(E)** 0.10 dpa (2×10^{14} ions/cm^2), **(F)** amorphized at 0.30 dpa (6.25×10^{14} ions/cm^2); irradiation process of $KLuTa_2O_7/K_{0.4}Lu_{0.8}Ta_2O_{6.4}$: **(G)** unirradiated, **(H)** 0.07 dpa (1.5×10^{14} ions/cm^2), **(I)** amorphized at 0.14 dpa (3×10^{14} ions/cm^2).

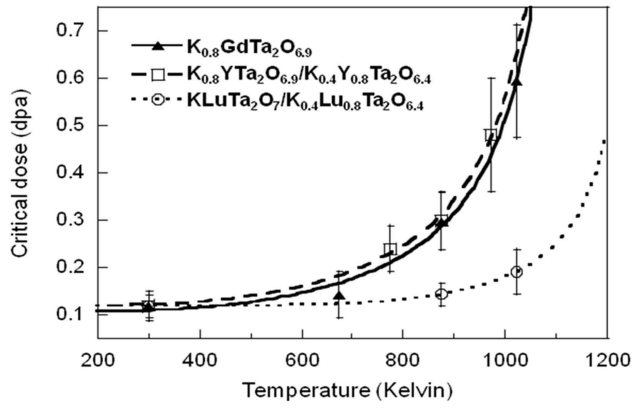

FIGURE 5 | Temperature dependence of the critical amorphization dose of the $K_xLn_yTa_2O_{7-v}$ samples.

temperature. At 873 K, the critical doses of both $K_{0.8}GdTa_2O_{6.9}$ and $K_{0.8}YTa_2O_{6.9}/K_{0.4}Y_{0.8}Ta_2O_{6.4}$ increase to ~0.30 dpa; in contrast, the critical dose of $KLuTa_2O_7/K_{0.4}Lu_{0.8}Ta_2O_{6.4}$ only slightly increases to 0.14 dpa. The difference becomes even larger at higher temperatures, indicating different dynamics of defect annealing.

The temperature dependence of radiation damage-induced amorphization of the nano-sized tantalate pyrochlores $K_xLn_yTa_2O_{7-v}$ upon 1 MeV Kr^{2+} irradiation is fitted with the following equation derived based on the direct-impact model:

$$D_c = \frac{D_0}{1 - \exp\left[\left(E_a/k\right)\left(1/T_c - 1/T\right)\right]} \quad (1)$$

where D_0 is the critical amorphization dose obtained by extrapolating the amorphization dose at $T = 0$ K; E_a is the dynamic annealing activation energy; T_c is the critical amorphization temperature above which the radiation-induced amorphization cannot occur (Weber et al., 1994; Wang et al., 1998, 2001). The fitted curve is shown in **Figure 5**. Based on the temperature dependence fitting, the critical amorphization temperatures, above which complete amorphization cannot be achieved, are 1167 ± 41 K for $K_{0.8}GdTa_2O_{6.9}$, 1165 ± 34 K for $K_{0.8}YTa_2O_{6.9}/K_{0.4}Y_{0.8}Ta_2O_{6.4}$, and ~1291 K for $KLuTa_2O_7/K_{0.4}Lu_{0.8}Ta_2O_{6.4}$.

COMPOSITION DEPENDENCE OF RADIATION TOLERANCE

Table 3 summarizes the nuclear and electron stopping power (S_n and S_e) of 1 MeV Kr^{2+} in the different tantalate pyrochlore samples, and their 48f oxygen x parameters (Wyckoff position), critical amorphization doses, and critical temperatures (T_c), which clearly show the higher radiation tolerance of $K_{0.8}GdTa_2O_{6.9}$ and $K_{0.8}YTa_2O_{6.9}/K_{0.4}Y_{0.8}Ta_2O_{6.4}$ than $KLuTa_2O_7/K_{0.4}Lu_{0.8}Ta_2O_{6.4}$. The x parameters of 48f oxygen Wyckoff positions indicate that the special atom positions in a crystal. Since $K_{0.4}Y_{0.8}Ta_2O_{6.4}$ and $K_{0.4}Lu_{0.8}Ta_2O_{6.4}$ have small x parameters of 48f oxygen (0.305 and 0.306, respectively) and thus are closer to the $A_2B_2O_6$ defect pyrochlore structure, they have larger deviation from the parent fluorite structure-type as compared with the $A_2B_2O_7$-based $K_{0.8}YTa_2O_{6.9}$ ($x = 0.332$) and $KLuTa_2O_7$ ($x = 0.316$) phases. Previous results on a wide range of pyrochlore compositions indicated that materials become more sensitive to radiation damage with increasing structural deviations from the parent fluorite structure, as evidenced by the lower 48f oxygen positional parameter (Lian et al., 2002). Therefore, $K_{0.8}YTa_2O_{6.9}$ and $KLuTa_2O_7$ with compositions close to $A_2B_2O_7$ with greater 48f oxygen positional parameter may be more radiation tolerant, which may determine the overall critical amorphization doses of the dual-phase $K_{0.8}YTa_2O_{6.9}/K_{0.4}Y_{0.8}Ta_2O_{6.4}$ and $KLuTa_2O_7/K_{0.4}Lu_{0.8}Ta_2O_{6.4}$, respectively. Therefore, we only consider the phases of $K_{0.8}GdTa_2O_{6.9}$, $K_{0.8}YTa_2O_{6.9}$, and $KLuTa_2O_7$ in the following discussion of composition dependence of radiation tolerance.

The greater radiation susceptibility to radiation-induced amorphization for $KLuTa_2O_7$ as compared with $K_{0.8}GdTa_2O_{6.9}$ and $K_{0.8}YTa_2O_{6.9}$ may be attributed to the variation in K^+ content, resulting in the change of cation ionic radius ratio and structural deviation from the parent fluorite structure, and thus, affecting their radiation performance. Particularly, the A and B site ionic radius ratio is critical in determining the radiation tolerance of $A_2B_2O_7$ pyrochlores, as a larger r_A/r_B ratio can lead to an increase in the A–B anti-site defect formation energy (Sickafus et al., 2000). Consequently, the structure is less capable of accommodating the high-displacement defects created by the incident ions, leading to lower amorphization resistance. In these $K_xLn_yTa_2O_{7-v}$ samples, K^+/Ta^{5+} has the largest r_A/r_B ratio of 2.359, significantly larger than those of Gd^{3+}/Ta^{5+} (1.645), Y^{3+}/Ta^{5+} (1.592), and Lu^{3+}/Ta^{5+} (1.526). Due to the prominently large ionic radius ratio of K^+/Ta^{5+}, the K^+ cation in the tantalate pyrochlores may dominate the structural deviation of pyrochlores, which controls their radiation tolerance. Our ion irradiation experiments show that $K_{0.8}GdTa_2O_{6.9}$ and $K_{0.8}YTa_2O_{6.9}$, both having lower K^+ occupancy at A-site, are less sensitive to the radiation-induced amorphization at elevated temperature with relatively lower critical amorphization temperature; in contrast, the K^+-rich $KLuTa_2O_7$ sample is more sensitive to the radiation-induced amorphization, and thus, has much higher critical temperature.

The lower amorphization doses and higher critical amorphization temperatures of these K^+-doped tantalate pyrochlore samples as compared with the non-K^+-doped titanate and zirconate pyrochlores indicate that the tantalate pyrochlores used in our study may be more susceptible to radiation-induced amorphization. The doping of K^+ cations with large ionic radius may be responsible, at least partially, for the more radiation-sensitive nature of these tantalate pyrochlores as compared to non-K^+-doped rare earth titanate (Lian et al., 2003), zirconate (Lian et al., 2002), and stannate pyrochlores (Lian et al., 2006) with smaller r_A/r_B. The correlation of the critical amorphization temperature T_c with the A–B site ionic ratio r_A/r_B of pyrochlores is discussed based on our radiation data of nano-sized tantalate pyrochlore and the previous radiation data of various bulk titanate and zirconate pyrochlores (Lian et al., 2002, 2003), as shown in **Figure 6**. Since we have demonstrated above that the chemical composition effect may overwhelm the size effect and significantly reduce the radiation tolerance of pyrochlore, bulk tantalate

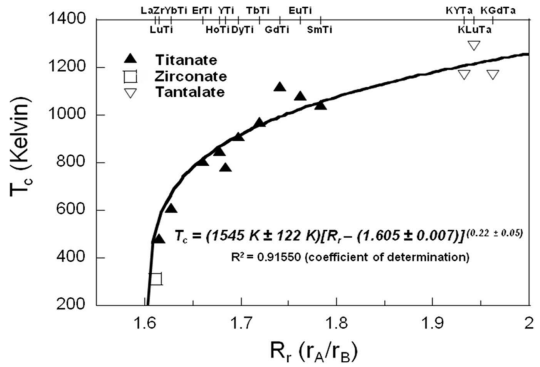

FIGURE 6 | Correlation of A–B site ionic radius ratio (r_A/r_B) with critical amorphization temperature (T_c) for titanate and zirconate $A_2B_2O_7$ pyrochlores and tantalate $K_xLn_yTa_2O_{7-v}$ pyrochlores. The different cation compositions of these pyrochlores are indicated in the upper *x*-axis, where the titanate and zirconate pyrochlores are indicated by the A and B site cations in the form of "A–B," and the tantalate pyrochlores are indicated by "KGdTa" (representing $K_{0.8}GdTa_2O_{6.9}$), "KYTa" (representing $K_{0.8}YTa_2O_{6.9}$), and "KLuTa" (representing $KLuTa_2O_7$). The empirical power-law fitting equation of $T_c = (1545 \pm 122\ K)\ [R_r - (1.605 \pm 0.007)]^{(0.22 \pm 0.05)}$ and the R^2 of fitting (coefficient of determination) is given at the lower right of the figure.

pyrochlores with the same chemical compositions may possess similar or slightly lower T_c, which will only have a minor impact on the correlation curve in **Figure 6**. For the tantalate pyrochlore phases of $K_{0.8}GdTa_2O_{6.9}$, $K_{0.8}YTa_2O_{6.9}$, and $KLuTa_2O_7$, whose A-sites are occupied by both K and Ln (Ln = Gd, Y, and Lu), the r_A/r_B values are determined by using the average r_A/r_B values weighted by the A-site occupancy of K and Ln. The resulting r_A/r_B versus T_c curve exhibits a near power-law relationship, which can be well fitted based on an empirical power-law function in the form of $T_c = T_0\ (R_r - R_{rc})^n$, where R_r is defined as the r_A/r_B radius ratio, R_{rc} is defined as the threshold of r_A/r_B value at which T_c approaches absolute 0, and T_0 is a temperature constant in Kelvin and n is the exponent constant. The best fitting of the experimental data is $T_c = (1545 \pm 122\ K)[R_r - (1.605 \pm 0.007)]^{(0.22 \pm 0.05)}$ with $R^2 = 0.91550$ (coefficient of determination), indicating that the threshold of r_A/r_B value locates at 1.605 ± 0.007 (R_{rc}) and the exponent constant $n = 0.22 \pm 0.05$. This result is consistent with previous radiation experiments on zirconate pyrochlores, in which $La_2Zr_2O_7$ ($r_A/r_B = 1.611$), whose r_A/r_B value is above the 1.605 ± 0.007 threshold, can be amorphized by 1.5 MeV Kr^{2+}; whereas $Nd_2Zr_2O_7$ ($r_A/r_B = 1.540$), $Sm_2Zr_2O_7$ ($r_A/r_B = 1.497$), and $Gd_2Zr_2O_7$ ($r_A/r_B = 1.462$) with r_A/r_B values below 1.605 ± 0.007 cannot be amorphized even at low temperatures. The prediction is also consistent with a previous model based on the electronic bonding calculation developed by Lumpkin et al. to predict the radiation tolerance of synthetic pyrochlores (Lumpkin et al., 2007). In general, K^+ content at the A sites of tantalate pyrochlores will result in an increase of the r_A/r_B value, which in turn can significantly reduce their radiation stability, highlighting important implication of chemical composition control for designing radiation resistant materials for nuclear waste forms and fuel matrix applications.

CONCLUSION

The radiation response of nano-sized (~10–15 nm) tantalate pyrochlores $K_xLn_yTa_2O_{7-v}$ (Ln = Gd, Y, and Lu) was investigated using 1 MeV Kr^{2+} ion beam irradiations at different temperatures, and the cation composition dependence of the ion beam-induced amorphization was studied. EDS measurements and XRD refinement reveal that the Y^{3+} and Lu^{3+}-doped pyrochlore samples are dual-phase as $K_{0.8}YTa_2O_{6.9}/K_{0.4}Y_{0.8}Ta_2O_{6.4}$ and $KLuTa_2O_7/K_{0.4}Lu_{0.8}Ta_2O_{6.4}$, respectively; whereas a single phase of $K_{0.8}GdTa_2O_7$ exists in the Gd^{3+}-doped tantalate pyrochlore. Ion beam-induced amorphization processes were observed in these nano-sized $K_xLn_yTa_2O_{7-v}$ by *in situ* TEM. At elevated temperatures, both $K_{0.8}GdTa_2O_7$ and $K_{0.8}YTa_2O_{6.9}/K_{0.4}Y_{0.8}Ta_2O_{6.4}$ exhibit higher radiation tolerance than $KLuTa_2O_7/K_{0.4}Lu_{0.8}Ta_2O_{6.4}$, and the critical temperatures of $K_{0.8}GdTa_2O_7$ and $K_{0.8}YTa_2O_{6.9}/K_{0.4}Y_{0.8}Ta_2O_{6.4}$ are estimated to be 1167 ± 41 and 1165 ± 34 K, respectively, lower than that of $KLuTa_2O_7/K_{0.4}Lu_{0.8}Ta_2O_{6.4}$ (~1291 K). Compared with $K_{0.4}Y_{0.8}Ta_2O_{6.4}$ and $K_{0.4}Lu_{0.8}Ta_2O_{6.4}$ who are close to the $A_2B_2O_6$ defect pyrochlore structure, the $K_{0.8}GdTa_2O_7$, $K_{0.8}YTa_2O_{6.9}$, and $KLuTa_2O_7$ phases, having less structural deviation from the parent fluorite structure, may be responsible for the overall radiation tolerance. The less radiation tolerance of $KLuTa_2O_7$ as compared to $K_{0.8}GdTa_2O_7$ and $K_{0.8}YTa_2O_{6.9}$ is attributed to the high K^+ occupancy at pyrochlore A sites in $K_xLn_yTa_2O_{7-v}$, resulted from the prominently large ionic radius ratio of K^+/Ta^{5+} and consequently the large anti-site defect formation energy. An empirical threshold ionic radius ratio (r_A/r_B) of 1.605 ± 0.007 is determined by analyzing the radiation data of these tantalate pyrochlores and the previous data of titanate and zirconate pyrochlores. Pyrochlores with r_A/r_B smaller than 1.605 ± 0.007 are extremely resistant to displacive radiation-induced amorphization. The radiation-sensitive nature of the nano-sized $K_xLn_yTa_2O_{7-v}$ tantalate pyrochlores may also be due to the rich K^+ content, as it significantly increases the average r_A/r_B value. These results highlight that the radiation tolerance of nanostructured materials is highly compositional dependent, and nano-sized tantalate pyrochlores are sensitive to radiation damage.

ACKNOWLEDGMENTS

This work was supported by a NSF career award DMR 1151028. We thank the staff of the IVEM-tandem Facility at the Argonne National Laboratory for assistance with the irradiation experiments. We also acknowledge Dr. May Nyman of Sandia National Laboratory in providing tantalate pyrochlores samples for radiation study.

REFERENCES

Ewing, R. C., Weber, W. J., and Lian, J. (2004). Nuclear waste disposal-pyrochlore $A_2B_2O_7$: nuclear waste form for the immobilization of plutonium and "minor" actinides. *J. Appl. Phys.* 95, 5949. doi:10.1063/1.1707213

Lian, J., Chen, J., Wang, L. M., Ewing, R. C., Farmer, J. M., Boatner, L. A., et al. (2003). Radiation-induced amorphization of rare-earth titanate pyrochlores. *Phys. Rev. B* 68, 134107. doi:10.1103/PhysRevB.68.134107

Lian, J., Helean, K. B., Kennedy, B. J., Wang, L. M., Navrotsky, A., and Ewing, R. C. (2006). Effect of structure and thermodynamic stability on the response of lanthanide stannate-pyrochlores to ion beam irradiation. *J. Phys. Chem. B* 110, 2343. doi:10.1021/jp055266c

Lian, J., Zu, X. T., Kutty, K. V. G., Chen, J., Wang, L. M., and Ewing, R. C. (2002). Ion-irradiation-induced amorphization of $La_2Zr_2O_7$ pyrochlore. *Phys. Rev. B* 66, 054108. doi:10.1103/PhysRevB.66.054108

Lumpkin, G. R., Pruneda, M., Rios, S., Smith, K. L., Trachenko, K., Whittle, K. R., et al. (2007). Nature of the chemical bond and prediction of radiation tolerance in pyrochlore and defect fluorite compounds. *J. Solid State Chem.* 180, 1512. doi:10.1016/j.jssc.2007.01.028

Nyman, M., Rodriguez, M. A., Shea-Rohwer, L. E., Martin, J. E., and Provencio, P. P. (2009). Highly versatile rare earth tantalate pyrochlore nanophosphors. *J. Am. Chem. Soc.* 131, 11652. doi:10.1021/ja903823w

Patel, M. K., Vijayakumar, V., Avasthi, D. K., Kailas, S., Pivin, J. C., Grover, V., et al. (2008). Effect of swift heavy ion irradiation in pyrochlores. *Nucl. Instrum. Methods Phys. Res. B* 266, 2898. doi:10.1016/j.nimb.2008.03.135

Raison, P. E., Haire, R. G., Sato, T., and Ogawa, T. (1999). Fundamental and technological aspects of actinide oxide pyrochlores: relevance for immobilization matrices. *Mater. Res. Soc. Symp. Proc.* 556, 3. doi:10.1557/PROC-556-3

Rose, M., Balogh, A. G., and Hahn, H. (1997). Instability of irradiation induced defects in nanostructured materials. *Nucl. Instrum. Methods Phys. Res. B* 127, 119. doi:10.1016/S0168-583X(96)00863-4

Rose, M., Gorzawski, G., Miehe, G., Balogh, A. G., and Hahn, H. (1995). Phase stability of nanostructured materials under heavy ion irradiation. *Nanostruct. Mater.* 6, 731. doi:10.1088/0957-4484/20/24/245303

Shen, T. D., Feng, S., Tang, M., Valdez, J. A., Wang, Y., and Sickafus, K. E. (2007). Enhanced radiation tolerance in nanocrystalline $MgGa_2O_4$. *Appl. Phys. Lett.* 90, 263115. doi:10.1063/1.2753098

Sickafus, K. E., Minervini, L., Grimes, R. W., Valdez, J. A., Ishimaru, M., Li, F., et al. (2000). Radiation tolerance of complex oxides. *Science* 289, 748. doi:10.1126/science.289.5480.748

Subramanian, A., Aravamudan, G., and Rao, G. V. S. (1983). Oxide pyrochlores – a review. *Prog. Solid. State Chem.* 15, 55. doi:10.1039/b904702f

Wang, H., Araujo, R., Swadener, J. G., Wang, Y. Q., Zhang, X., Fu, E. G., et al. (2007). Ion irradiation effects in nanocrystalline TiN coatings. *Nucl. Instrum. Methods Phys. Res. B* 261, 1162. doi:10.1016/j.nimb.2007.04.248

Wang, S. X., Begg, B. D., Wang, L. M., Ewing, R. C., Weber, W. J., and Kutty, K. V. G. (1999). Radiation stability of gadolinium zirconate: a waste form for plutonium disposition. *J. Mater. Res.* 14, 4470. doi:10.1557/JMR.1999.0606

Wang, S. X., Wang, L. M., and Ewing, R. C. (1998). A model for irradiation-induced amorphization. *Mater. Res. Soc. Symp. Proc.* 504, 165. doi:10.1557/PROC-504-165

Wang, S. X., Wang, L. M., and Ewing, R. C. (2001). Irradiation-induced amorphization: effects of temperature, ion mass, cascade size, and dose rate. *Phys. Rev. B* 63, 024105. doi:10.1103/PhysRevB.63.024105

Weber, W. J., Ewing, R. C., and Wang, L. M. (1994). The radiation-induced crystalline-to-amorphous transition in zircon. *J. Mater. Res.* 9, 688. doi:10.1557/JMR.1994.0688

Zhang, J. M., Lian, J., Fuentes, A., Zhang, F. X., Lang, M., Lu, F. Y., et al. (2009a). Enhanced radiation resistance of nanocrystalline pyrochlore $Gd_2(Ti_{0.65}Zr_{0.35})_2O_7$. *Appl. Phys. Lett.* 94, 243110. doi:10.1063/1.3155855

Zhang, Z. L., Xiao, H. Y., Zu, X. T., Gao, F., and Weber, W. J. (2009b). First-principles calculation of structural and energetic properties for $A_2Ti_2O_7$ (A = Lu, Er, Y, Gd, Sm, Nd, La). *J. Mater. Res.* 24, 1335. doi:10.1557/jmr.2009.0152

Zhang, J. M., Lian, J., Zhang, F. X., Wang, J. W., Fuentes, A. F., and Ewing, R. C. (2010). Intrinsic Structural disorder and radiation response of nanocrystalline Gd-$_2(Ti_{0.65}Zr_{0.35})_2O_7$ pyrochlore. *J. Phys. Chem. C* 114, 11810. doi:10.1021/jp103371j

Conflict of Interest Statement: The authors declare that the research was conducted in the absence of any commercial or financial relationships that could be construed as a potential conflict of interest.

Received: 16 August 2014; accepted: 15 October 2014; published online: 31 October 2014.

*Citation: Lu F, Shen Y, Dong Z, Wang G, Zhang F, Ewing RC and Lian J (2014) Ion beam irradiation-induced amorphization of nano-sized $K_xLn_yTa_2O_{7-v}$ tantalate pyrochlore. Front. Energy Res. **2**:48. doi: 10.3389/fenrg.2014.00048*

This article was submitted to Nuclear Energy, a section of the journal Frontiers in Energy Research.